IMA Journal of Applied Mathematics (2017) **82**, 280–304
doi:10.1093/imamat/hxw038
Advance Access Publication on 1 September 2016

An analytic solution for gust-aerofoil interaction noise including effects of geometry

This paper is a contribution by a finalist of the Lighthill-Thwaites 2015 Competition

Lorna J. Ayton
Department of Applied Mathematics and Theoretical Physics, University of Cambridge, Wilberforce Road, Cambridge CB3 0WA, UK
L.J.Ayton@damtp.cam.ac.uk

[Received on 17 November 2015; revised on 21 April 2016; accepted on 10 July 2016]

An analytic solution is obtained for the sound generated by gust-aerofoil interaction for aerofoils with thickness, camber and angle of attack. The model is based on the linearization of the Euler equations about a steady subsonic flow, and is an extension of previous work which considered restrictive aerofoil geometries. Only high-frequency incident gusts are considered. The aerofoil thickness, camber and angle of attack are such that the steady flow past the aerofoil is seen as a small perturbation to uniform flow. The method of matched asymptotic expansions is used to identify regions around the aerofoil where different processes govern the generation or propagation of sound. Key local regions at the leading and trailing edges of the aerofoil determine the generation of noise whilst transition regions along the rigid aerofoil surface, and outer regions away from the surface play key roles in the propagation of sound. The effects of varying thickness and camber angle are discussed, along with the effects of varying the radius of the leading edge.

Keywords: gust-aerofoil interaction; leading-edge noise; asymptotic analysis; Wiener–Hopf method.

1. Introduction

Aerofoil leading-edge noise, that is the generation of sound by the interaction of an unsteady vortical perturbation from far upstream with an aerofoil in steady flow, is one of the key sources of noise emitted by aeroengines. It arises due to vortical wakes shed from rotor blades interacting with downstream stator blades, in background flow, in a process known as gust-aerofoil interaction. Due to increasingly tight noise restrictions placed on the aviation industry, it is vital to have a qualitative and quantitative understanding of the noise generated by these blade–blade interactions, to then shed light on what can be done to reduce this noise.

In background uniform flow, gust-aerofoil interaction has received a great deal of interest both analytically (Myers & Kerschen, 1995, 1997; Tsai, 1992), and numerically (Hixon *et al.*, 2006; Gill *et al.*, 2013); however both approaches have their limitations. Numerical schemes typically focus on low- to mid-frequency range interactions, or limit aerofoil geometry by, e.g. ignoring camber. Conversely the analytic work obtains asymptotic solutions to the rapid distortion theory equations (Goldstein, 1978) only at high frequencies; Myers & Kerschen (1995, 1997) discuss the effects of camber and loading for zero-thickness plates, whilst Tsai (1992) discusses the effects of thickness for symmetric (i.e. uncambered) aerofoils.

Here we shall obtain an analytic solution for high-frequency gust-aerofoil interaction that allows for variations in camber, angle of attack and thickness, which can then be used as a test case for high-frequency numerical models that deal with full geometry, or could be implemented into a hybrid model for

fully turbulent interaction problems. We extend the analytically-based procedure of Myers & Kerschen (1995, 1997) and Tsai (1992) to study the full geometry gust-aerofoil interaction problem. We consider a high-frequency incident gust interacting with an aerofoil in steady uniform background flow, and use the following asymptotic limits; $k \gg 1$ is the acoustic reduced frequency; $\varepsilon \ll 1$ is a non-dimensionalized small parameter (lengths are non-dimensionalized with respect to semi-chord length) such that $t = \varepsilon t'$ and $\alpha = \varepsilon\alpha'$ are the thickness and camber, respectively, of the aerofoil; and we impose that $\varepsilon k = O(1)$. Results will be shown specifically for NACA 4-digit series aerofoils, however the final results will hold for any aerofoil with a parabolic leading edge. We also discuss how the results are expected to change for aerofoils with different leading-edge profiles; experimentally Chaitanya *et al.* (2015) have found that a larger leading-edge radius could result in a lower level of generated noise.

The method of matched asymptotic expansions (Van Dyke, 1975) is used to split the problem into various asymptotic regions around the aerofoil; the inner leading- and trailing-edge regions, of size $O(k^{-1})$ centred on the leading and trailing edges, respectively; the transition regions on the aerofoil surfaces between the inner leading- and trailing-edge regions, of width $O(k^{-1/2})$, which account for the surface curvature of the aerofoil; a wake region, also of width $O(k^{-1/2})$; and the outer region comprising the rest of space. The solution in each region is determined individually, and matched to its neighbouring regions using Van Dyke's matching rule (Van Dyke, 1975). An advantage of this analytical approach is that it provides results in the high-frequency regime (where numerical approaches become more difficult) as well as providing interesting physical insight.

The outline of this article is as follows; in Section 2 we formulate the mathematical problem leading to the governing equations. Section 3 discusses the solution in the leading-edge inner region, with Sections 3.1 and 3.3 specifically discussing the effects of an arbitrary leading-edge geometry. Section 4 discusses the outer solutions. In Section 5 the leading-edge transition solution is obtained, and the trailing-edge solutions are discussed in Section 6. In Section 7 the total far-field acoustic potential generated by gust-aerofoil interaction is given. Results are presented in Section 8 and we discuss conclusions in Section 9.

2. Formulation of problem

2.1. *Aerofoil geometry and steady mean flow*

We consider a small unsteady perturbation to the mean flow around a thin aerofoil of chord length $2b^*$ in Cartesian coordinates (x^*, y^*) with origin at the leading edge, where * denotes dimensional quantities. The thickness and camber of the aerofoil are small, $O(\varepsilon)$, and we restrict the geometry of the aerofoil to have a parabolic nose $(\varepsilon y^*(x^*) \sim 2a\varepsilon t'\sqrt{x^*/b^*}$, where $t = \varepsilon t'$ is the maximum thickness of the aerofoil and primed quantities are $O(1)$) and a sharp trailing edge. We decompose the boundary description of the aerofoil, $\varepsilon y^*(x^*)$, into thickness related terms, $\varepsilon y^{(t)*}$, camber and angle of attack related terms, $\varepsilon Y^{(c)*}(x^*) = -\alpha_i x^* + \varepsilon y^{(c)*}(x^*)$, where α_i is the angle of attack, and $y^{(c)}$ describes the camber line of the aerofoil.

In what follows we non-dimensionalize lengths with respect to b^*, and velocities by U^*_∞, where U^*_∞ is the uniform mean flow speed far upstream. We proceed to analyse the mean flow in the same manner as the sound-aerofoil interaction problem (Ayton & Peake, 2013). For clarity the key steps are repeated here.

We work in the non-dimensionalized orthogonal coordinate system (ϕ, ψ), given by the velocity potential and streamfunction of the mean flow around the aerofoil. In this coordinate system we write $z = \phi + i\psi$, which relates to the Cartesian coordinates (x, y) via

$$x + i\beta_\infty y = z + O(\varepsilon), \tag{2.1}$$

where $\beta_\infty^2 = (1 - M_\infty^2)$ is the Prandtl–Glauert transformation factor accounting for compressibility, and M_∞ is the mean flow Mach number at upstream infinity.

To utilize the modified rapid distortion theory equations determined by Kerschen & Myers (1987), we need the complex potential for the steady flow around the aerofoil. Using Thwaites (1960) we find that, for a thin aerofoil, the amplitude of the total mean flow is $U_\infty^*(1 + \varepsilon q)$, in the direction making an angle $\varepsilon\mu$ with the x^* axis, where

$$(q - i\mu)(z) = \frac{1}{\pi\beta_\infty}\int_0^2 \frac{y^{(t)\prime}(x)}{z - x}\,\mathrm{d}x + \frac{1}{\pi\beta_\infty}\sqrt{\frac{2-z}{z}}\int_0^2 \frac{Y^{(c)\prime}(x)}{z-x}\sqrt{\frac{x}{2-x}}\,\mathrm{d}x, \tag{2.2}$$

and $'$ denotes differentiation. This is correct to first order in aerofoil thickness, camber and angle of attack. The quantities q and μ are related to the complex potential F (which is non-dimensionalized with respect to $U_\infty^{*2}b^*$) by

$$q(\phi, \psi) - i\mu(\phi, \psi) = \frac{\mathrm{d}F}{\mathrm{d}z}, \tag{2.3}$$

where the arbitrary constant in F is chosen so that $F(0) = 0$. This now completes the relation given by (2.1); the $O(\varepsilon)$ perturbation is $\varepsilon F(z)$. For further details of the coordinate transformation between physical (x, y)-space, and potential-streamline space, see Myers (1987).

We combine the angle of attack, $\alpha_i = \varepsilon\alpha_i'$, and the leading-edge camber together to give an effective angle of attack, $\alpha_{\mathrm{eff}} = \varepsilon\alpha_{\mathrm{eff}}'$, with

$$\alpha_{\mathrm{eff}} = \alpha_i - \frac{1}{\pi}\int_0^2 \frac{\varepsilon y^{(c)}(x)(1-x)}{((2-x)x)^{3/2}}\,\mathrm{d}x. \tag{2.4}$$

We may therefore expand $q - i\mu \sim \alpha_{\mathrm{eff}}'\beta_\infty^{-1}\sqrt{2}z^{-1/2} + \text{thickness term} + O(z^{1/2})$ close to the leading edge. The complex velocity potential for a general thin aerofoil with boundary $\varepsilon y(x) = \varepsilon y^{(t)}(x) + \varepsilon y^{(c)}(x)$, where t and c denote thickness and camber, respectively, can be written as $F = F_0 + F^{(t)} + F^{(c)}$, where F_0 is the flat-plate potential at angle of attack α_i as given in Myers & Kerschen (1995). The flat-plate (at the angle of attack), thickness and camber dependent components of the complex potential are given by

$$F_0(z) = \frac{i\alpha_i}{\beta_\infty}\left(\log\left[z - 1 + \sqrt{z(z-2)}\right] + z - \sqrt{z(z-2)} - \pi i\right), \tag{2.5}$$

$$F^{(t)}(z) = \frac{1}{\pi\beta_\infty}\left(\int_0^2 y^{(t)\prime}(x)\log[z-x]\,\mathrm{d}x + \int_0^2 \frac{y^{(t)\prime}(x)}{x}\,\mathrm{d}x\right), \tag{2.6}$$

$$F^{(c)}(z) = \frac{-i}{\pi\beta_\infty}\int_0^2 y^{(c)\prime}(x)\frac{\sqrt{x}}{\sqrt{2-x}}\left(\log\left[\frac{1+\sqrt{(z-2)/z}}{1-\sqrt{(z-2)/z}}\right] - i\frac{\sqrt{2-x}}{\sqrt{x}}\log\left[\frac{i\sqrt{(2-x)/x}+\sqrt{(z-2)/z}}{i\sqrt{(2-x)/x}-\sqrt{(z-2)/z}}\right] - \pi i\right)\mathrm{d}x. \tag{2.7}$$

This completes our description of the mean flow.

A shift of $z \to z + 2$ reformulates these expressions for use at the trailing edge (with constant then chosen such that $F_t(z_t = 0) = 0$), which will be required in Sections 4 and 6.

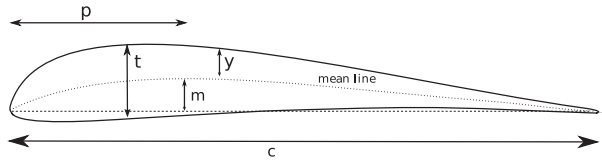

Fig. 1. NACA 4-digit series aerofoil.

For the purposes of this article we shall focus on the NACA 4-digit series of aerofoils, as illustrated in Fig. 1. The equation of the boundary of a general NACA 4-digit series aerofoil is given by

$$y_{\pm} = y^{(c)} \pm y^{(t)} \cos\chi, \tag{2.8a}$$

where $\pm$ denotes the upper or lower arc, respectively. We define $y^{(c)}$, $y^{(t)}$ and χ by

$$y^{(c)} = \begin{cases} \frac{mx}{p^2}(2p - \frac{x}{2}) & 0 \le x \le 2p \\ \frac{m(2-x)}{(1-p)^2}(1 + \frac{x}{2} - 2p) & 2p \le x \le 2 \end{cases}, \tag{2.8b}$$

$$y^{(t)} = \frac{t}{0.1}(a_1\sqrt{\frac{x}{2}} - a_2\frac{x}{2} - a_3\frac{x^2}{2^2} + a_4\frac{x^3}{2^3} - a_5\frac{x^4}{2^4}), \tag{2.8c}$$

$$\chi = \arctan\frac{\mathrm{d}y^{(c)}}{\mathrm{d}x}, \tag{2.8d}$$

with

$$a_1 = 0.2969, \qquad a_2 = 0.1260, \qquad a_3 = 0.3516, \qquad a_4 = 0.2843, \qquad a_5 = 0.1036. \tag{2.8e}$$

Note the standard choice of a_5 is 0.1015 however we wish to consider a sharp trailing edge, $y^{(t)}(2) = 0$, hence the variation. Here, the non-dimensionalized chord length is 2, x is the position along the chord, y is the half thickness at a given value of x from the centreline to the surface, and t is the maximum thickness as a percentage of the chord. m is the maximum camber and p is the location of the maximum camber along the centreline, both given as percentages of the total chord length. A NACA 4-digit series aerofoil is defined by p, m and t: $100m$ gives the first digit, $10p$ gives the second digit and $100t$ gives the last two digits.

We will discuss aerofoils with different leading-edge profiles although we will not explicitly calculate the total far-field scattered noise in this arbitrary case.

2.2. *Unsteady disturbance equations*

Rapid distortion theory is often used to investigate the sound generated by the interaction of an unsteady flow with a solid boundary. The theory was initially developed by Hunt (1973) and Goldstein (1978) for 3D incompressible and compressible flows, respectively, but the form given by Kerschen & Myers (1987) and Kerschen & Balsa (1981) for 2D, small-disturbance mean flows is more relevant to this article. We assume that the fluid is inviscid and non-heat conducting. In our new coordinate system, the third, spanwise direction, is x_3 and we assume that all unsteady quantities are proportional to $\mathrm{e}^{ik_3x_3 - i\omega t}$, where

ω is the non-dimensionalized frequency. We non-dimensionalize coordinates (ϕ^*, ψ^*) with respect to $U_\infty^* b^*$, wavevector $\boldsymbol{k} = k^*(k_1, k_2, k_3)$ with respect to $(b^* U_\infty^*)^{-1}$ and frequency with respect to $k^* U_\infty^{*2}$.

A full derivation of the equations can be found in Tsai (1992) and Ayton (2014). Here we only repeat the key equations. Importantly the unsteady velocity field is separated into a (non-acoustic) gust component and an acoustic response. By evaluating the evolution of the incident gust in the steady flow of Mach number M_∞ around the aerofoil, we then determine an equation for the acoustic response with forcing arising due to the incident gust. Far upstream the incident gust takes the form $(A_t, A_n, A_3)\,\mathrm{e}^{ik(k_t\phi + k_n\psi + k_3 z - k_t t)}$, such that $A_t k_t + A_n k_n \beta_\infty + A_3 k_3 = 0$. The acoustic response is determined via the modified unsteady velocity potential, h which satisfies

$$\frac{\partial^2 h}{\partial \phi^2} + \frac{\partial^2 h}{\partial \psi^2} + k^2 w^2 (1 - 2\beta_\infty^2 \varepsilon q) h + \frac{(\gamma+1) M_\infty^4 \varepsilon q}{\beta_\infty^2}\left(\frac{\partial^2 h}{\partial \psi^2} + 2ik\delta \frac{\partial h}{\partial \phi} + k^2(w^2 + \delta^2) h\right) - \frac{(\gamma+1) M_\infty^4 \varepsilon}{\beta_\infty^2} \frac{\partial q}{\partial \phi}\left(\frac{\partial h}{\partial \phi} - ik\delta h\right) = k\varepsilon S(\phi, \psi)\,\mathrm{e}^{ik\Omega}, \quad (2.9a)$$

where

$$\delta = k_t/\beta_\infty^2, \qquad w^2 = (M_\infty \delta)^2 - (k_3/\beta_\infty)^2, \qquad \Omega = \delta\phi + k_n \psi + \varepsilon g(\phi, \psi), \quad (2.9b)$$

and the forcing arising from the evolution of the incident gust in the background flow is given by

$$S(\phi, \psi) = \frac{2}{\beta_\infty^2}\left(i(A_t - A_n k_n \beta_\infty^3) q + i(\beta_\infty^2 k_n A_t + A_n \beta_\infty)\mu + \frac{A_t M_\infty^2}{k}\frac{\partial q}{\partial \phi} + \frac{A_n M_\infty^2 \beta_\infty}{k}\frac{\partial q}{\partial \psi}\right). \quad (2.9c)$$

The function, $g(\phi, \psi)$, is Lighthill's drift function,

$$g(\phi, \psi) = -2\int_{-\infty}^{\phi} q(\eta, \psi)\,\mathrm{d}\eta, \quad (2.9d)$$

and the boundary condition of zero normal velocity on the solid surface is

$$\left.\frac{\partial h}{\partial \psi} + M_\infty^2 \varepsilon \frac{\partial q}{\partial \psi} h\right|_{\psi=0} = \left.\left(-\frac{A_n}{\beta_\infty} + 2\varepsilon\mu A_t + \frac{A_n M_\infty^2 \varepsilon q}{\beta_\infty}\right)\mathrm{e}^{ik\Omega}\right|_{\psi=0}. \quad (2.10)$$

We work with the modified unsteady pressure, as defined by Myers & Kerschen (1995, Equation (2.7)), which is given by

$$p = -\left(\frac{\partial h}{\partial \phi} - ik\delta h\right)\mathrm{e}^{-ik\delta M_\infty^2 \phi}. \quad (2.11)$$

We now use the method of matched asymptotic expansions (Van Dyke, 1975) to solve in all regions shown in Fig. 2 following a similar procedure as Myers & Kerschen (1995, 1997) and Tsai (1992). We begin with the leading-edge inner region, (i), then match to the outer region, (ii). The leading-edge transition region, (iii), along the aerofoil surface can then be constructed. A similar process is completed at the trailing edge. First the inner region, (iv), is found, then matched to the outer region, (ii), and finally a transition region, (v), is determined to ensure continuity of pressure across the wake. The trailing-edge solutions rely on the rescattering of the leading-edge solution by the trailing edge.

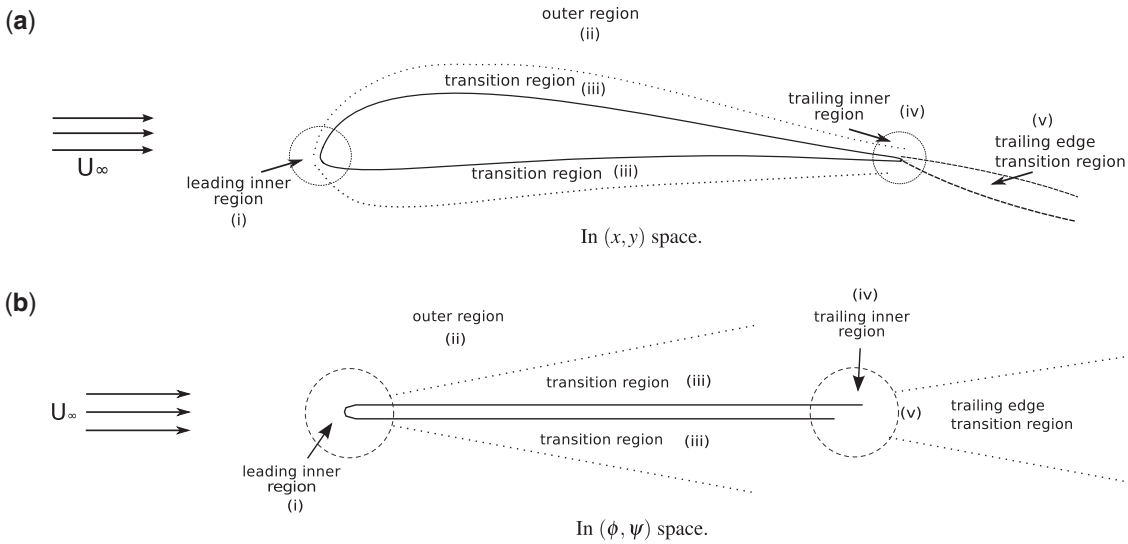

Fig. 2. Asymptotic regions around the aerofoil. (a) In (x, y) space. (b) In (ϕ, ψ) space; leading- and trailing-edge inner regions, (i) and (iv), scale as $O(k^{-1})$, and the width of the transition regions, (iii) scale as $O(k^{-1/2})$. The outer region (ii) is $O(1)$. We solve for (i) in Section 3, and solve for (ii) in Section 4. Region (iii) is solved for in Section 5, and regions (iv) and (v) are solved for in Sections 6.1 and 6.2, respectively.

3. Leading-edge inner solution

We move to inner variables, $(\Phi, \Psi) = k(\phi, \psi)$, to focus on region (i) illustrated in Fig. 2.

In the leading-edge region, the governing equation, (2.9a), becomes

$$\frac{\partial^2 H}{\partial \Phi^2} + \frac{\partial^2 H}{\partial \Psi^2} + w^2(1 - 2\beta_\infty^2 \varepsilon q)H + \frac{(\gamma+1)M_\infty^4}{\beta_\infty^2}\varepsilon q\left(\frac{\partial^2 H}{\partial \Psi^2} + 2i\delta\frac{\partial H}{\partial \Phi} + (w^2+\delta^2)H\right) - \frac{(\gamma+1)M_\infty^4}{\beta_\infty^2}\varepsilon\frac{\partial q}{\partial \Phi}\left(\frac{\partial H}{\partial \Phi} - i\delta H\right) = \frac{\varepsilon}{k}\,\mathrm{e}^{i\bar{\Omega}} S(\Phi, \Psi), \tag{3.1a}$$

$$\bar{\Omega} = \delta\Phi + k_n\Psi + k\varepsilon g(\Phi, \Psi), \tag{3.1b}$$

$$S(\Phi, \Psi) = \frac{2}{\beta_\infty^2}\left(iq(A_t^* - A_n k_n \beta_\infty^3) + i\beta_\infty\mu(\beta_\infty k_n A_t^* + A_n) + A_t^* M_\infty^2\frac{\partial q}{\partial \Phi} + A_n M_\infty^2 \beta_\infty \frac{\partial q}{\partial \Psi}\right), \tag{3.1c}$$

subject to boundary condition

$$\frac{\partial H}{\partial \Psi} + M_\infty^2 \varepsilon \frac{\partial q}{\partial \Psi} H\bigg|_{\Psi=0\pm} = \frac{1}{k}\left(-\frac{A_n}{\beta_\infty} + 2\varepsilon\mu A_t^* + \frac{A_n M_\infty^2 \varepsilon q}{\beta_\infty}\right)\mathrm{e}^{i\bar{\Omega}}\bigg|_{\psi=0}. \tag{3.2}$$

For a parabolic leading edge, the inner solution can be expanded as

$$H(\Phi, \Psi) = \frac{1}{k}\,\mathrm{e}^{2ik\varepsilon F_R(-\infty)}\left(H_0 + \varepsilon t'\sqrt{k}(H_1 + H_2 + H_3) + \varepsilon\alpha'_{\mathrm{eff}}\sqrt{k}(P_1 + P_2 + P_3) + O(\varepsilon)\right). \tag{3.3}$$

Recall $t = \varepsilon t'$ and $\alpha_{\text{eff}} = \varepsilon \alpha'_{\text{eff}}$ represent the thickness, camber and angle of attack parameters of the aerofoil, respectively, hence $H_{1,2,3}$ are thickness-dependent perturbations and $P_{1,2,3}$ are loading/camber-dependent perturbations. $F_R(-\infty)$ contains both thickness- and camber-dependent terms and is defined via $F_R(z) = \text{Re}(F(z))$.

Myers & Kerschen (1997) obtain an analytic solution for zero-thickness cambered plates at non-zero angle of attack, whilst Tsai (1992) obtains a solution for symmetric aerofoils with non-zero thickness at zero angle of attack. The camber-related leading-edge inner solution depends only on the local leading-edge camber distribution and therefore can be obtained directly from Myers & Kerschen (1997), however the thickness-related solution cannot be taken directly from Tsai (1992) since Tsai considered only Joukowski aerofoils whereas we allow for any thickness distribution subject to the constraint of a parabolic leading edge. Further, we have identified errors in Tsai's analysis which we correct in the following sections. For each term, $H_{0,1,2,3}$ and $P_{1,2,3}$ we also determine the outer limit, $\Phi, \Psi \gg 1$, of the inner solution to enable asymptotic matching to the outer solutions in Section 6.

3.1. *Effects of leading-edge geometry*

The asymptotic series (3.3) holds provided the leading edge has a parabolic geometry, $y \sim 2a\varepsilon t'\sqrt{x}$; it is this that determines the size of the asymptotic parameter, $\varepsilon\sqrt{k}$ in the correction terms, since $q = O(\sqrt{k})$ in the inner region. If however we allow an arbitrary leading-edge geometry, $y \sim 2a\varepsilon t' x^m$, in the inner region $q = O(k^{1-m})$ and the asymptotic parameter governing the size of the correction terms becomes εk^{1-m}. For thinner leading edges, i.e. $m \to 1$, the size of the correction terms are decreased as is expected since the level of horizontal blocking is also decreased with leading-edge radius.

3.2. *Solution for the flat-plate term H_0*

The blocking of the vertical component of the incident gust velocities is determined by H_0, which satisfies

$$D(H_0) = 0, \tag{3.4a}$$

$$\left.\frac{\partial H_0}{\partial \Psi}\right|_{\substack{\Phi>0 \\ \Psi=0}} = -\frac{A_n}{\beta_\infty} \mathrm{e}^{i\delta\Phi}, \tag{3.4b}$$

where D is the Helmholtz operator defined by $D = \frac{\partial^2}{\partial \Phi^2} + \frac{\partial^2}{\partial \Psi^2} + w^2$. We solve this using the Wiener–Hopf method, obtaining

$$H_0 = -\frac{A_n \,\text{sgn}(\Psi)}{\beta_\infty 2\pi\sqrt{\delta + w}} \int_{-\infty}^{\infty} \frac{\mathrm{e}^{-i\lambda\Phi - |\Psi|\sqrt{\lambda^2 - w^2}}}{(\lambda + \delta)\sqrt{\lambda + w}} \,\mathrm{d}\lambda. \tag{3.5}$$

The outer limit (obtained using the method of steepest descents) is given by

$$H_0 \sim L_0(\theta)\frac{\mathrm{e}^{ikwr}}{\sqrt{kr}} + O(k^{-3/2}), \tag{3.6a}$$

$$L_0(\theta) = -\frac{A_n \,\mathrm{e}^{-i\pi/4} \cos\theta/2}{\beta_\infty \sqrt{\pi}\sqrt{\delta + w}(\delta - w\cos\theta)}. \tag{3.6b}$$

This flat-plate solution is discussed in detail in Myers (1987) and Tsai (1992).

3.3. *Solution for thickness-related term H_1*

H_1 arises from the influence of aerofoil thickness on the surface boundary condition. In the case of a parabolic leading edge, $y \sim 2a\varepsilon t'\sqrt{x}$, H_1 satisfies

$$D(H_1) = 0, \tag{3.7a}$$

$$\left.\frac{\partial H_1}{\partial \Psi}\right|_{\substack{\Phi>0\\ \Psi=0\pm}} = \frac{2aA_t^*}{\beta_\infty\sqrt{\Phi}}\operatorname{sgn}(\Psi)\,\mathrm{e}^{i\delta\Phi}, \tag{3.7b}$$

which has solution

$$H_1 = -\frac{\mathrm{e}^{i\pi/4}A_t^* a}{\sqrt{\pi}\beta_\infty}\int_{-\infty}^{\infty}\frac{\mathrm{e}^{-i\lambda\Phi-|\Psi|\sqrt{\lambda^2-w^2}}}{\sqrt{\lambda^2-w^2}\sqrt{\lambda+\delta}}\,\mathrm{d}\lambda, \tag{3.8}$$

with outer limit

$$H_1 \sim L_1(\theta)\frac{\mathrm{e}^{ikwr}}{\sqrt{kr}} + O(k^{-3/2}), \tag{3.9a}$$

$$L_1(\theta) = -\frac{iA_t^* a\sqrt{2}}{\beta_\infty\sqrt{w}\sqrt{\delta - w\cos\theta}}. \tag{3.9b}$$

This is the generalized form of the H_1 solution presented in Tsai (1992).

In the case of an arbitrary leading edge, $y \sim 2a\varepsilon t' x^m$, the boundary condition (3.7b) becomes

$$\left.\frac{\partial H_1}{\partial \Psi}\right|_{\substack{\Phi>0\\ \Psi=0\pm}} = \frac{a}{\pi\beta_\infty m}\Gamma(1-m)\Gamma(1+m)\left[2A_t^*\sin(m\pi) - \frac{A_n M_\infty^2}{\beta_\infty}\cos(m\pi)\right]\frac{\mathrm{e}^{i\delta\Phi}}{\Phi^{1-m}} \tag{3.10}$$

$$\equiv \mathscr{C}(m)\frac{\mathrm{e}^{i\delta\Phi}}{\Phi^{1-m}}. \tag{3.11}$$

Therefore L_1 becomes

$$L_1(\theta) = \mathscr{C}(m)\frac{\Gamma(m)}{(\delta - w\cos\theta)^m}. \tag{3.12}$$

The remainder of our calculations will be done only for parabolic leading edges.

3.4. *Solution for thickness-related term H_2*

H_2 arises from the volume source terms in the local leading-edge region which come about due to the convected disturbance in the non-uniform flow around the nose. H_2 satisfies

$$D(H_2) = \mathrm{e}^{i\delta\Phi+ik_n\Psi}\left(\frac{C_1\cos,\theta/2 + C_2\sin\theta/2}{\sqrt{R}} + \frac{C_3\cos 3\theta/2 + C_4\sin 3\theta/2}{R^{3/2}}\right), \tag{3.13a}$$

$$\left.\frac{\partial H_2}{\partial \Phi}\right|_{\substack{\Phi>0\\ \Psi=0}} = 0, \tag{3.13b}$$

$$\begin{aligned} C_1 &= \frac{2ai}{\beta_\infty^2}(\beta_\infty k_n A_t^* + A_n), & C_2 &= -\frac{2ai}{\beta_\infty^3}(A_t^* - k_n A_n \beta_\infty^3),\\ C_3 &= -\frac{A_n M_\infty^2 a}{\beta_\infty^2}, & C_4 &= \frac{A_t^* M_\infty^2 a}{\beta_\infty^3}. \end{aligned} \tag{3.14}$$

This is now of the same form as the problem presented by Tsai (1992). We separate H_2 into complementary and particular solutions, H_{2c} and H_{2p}, respectively, and use Tsai's results now we have a problem of similar form. This results in outer solution;

$$H_2 \sim \frac{\mathrm{e}^{ik(\delta\phi + k_n\psi)}}{\sqrt{kr}}\left(\frac{C_1\cos\theta/2 + C_2\sin\theta/2}{\delta^2 + k_n^2 - w^2}\right) + L_2(\theta)\frac{\mathrm{e}^{ikwr}}{\sqrt{kr}} + O(k^{-3/2}), \tag{3.15a}$$

where

$$\begin{aligned} L_2(\theta) = {} & \frac{-i[(\delta - w\cos\theta)f_1(-w\cos\theta) + ik_n f_2(-w\cos\theta)]}{4\sqrt{2w}(\delta^2 + k_n^2)\sqrt{\delta - w\cos\theta}(\lambda_1 + w\cos\theta)(\lambda_2 + w\cos\theta)}\\ & - \frac{\cos\theta/2}{4(\lambda_1 - \lambda_2)(\delta^2 + k_n^2)}\left(4(\lambda_1 - \lambda_2)(i\delta C_3 + ik_n C_4) + \frac{\sqrt{\lambda_1 + w}f_2(\lambda_1)}{\sqrt{\lambda_1 + \delta}(\lambda_1 + x\cos\theta)}\right.\\ & \left. - \frac{(\lambda_2 + \delta)f_2(\lambda_2) + ik_n f_1(\lambda_2)}{(\lambda_2 + w\cos\theta)\sqrt{\lambda_2 - w}\sqrt{\lambda_2 + \delta}}\right), \end{aligned} \tag{3.15b}$$

and

$$f_1(\lambda) = (iC_2 - 2C_4(\lambda + \delta))(k_n^2 - \delta^2 - w^2 - 2\delta\lambda) + 2ik_n(\lambda + \delta)(C_1 + 2iC_3(\lambda + \delta)), \tag{3.15c}$$

$$f_2(\lambda) = 2ik_n(\lambda + \delta(iC_2 - 2C_4(\lambda + \delta)) + (C_1 + 2iC_3(\lambda + \delta))(k_n^2 - \delta^2 - w^2 - 2\delta\lambda), \tag{3.15d}$$

$$\lambda_{1,2} = -\frac{\delta}{2}\left(\frac{\delta^2 + k_n^2 + w^2}{\delta^2 + k_n^2}\right) \pm \frac{ik_n}{2}\left(\frac{\delta^2 + k_n^2 - w^2}{\delta^2 + k_n^2}\right). \tag{3.15e}$$

The first term in (3.15a) yields a hydrodynamic solution and arises from the particular solution, whilst the second is an acoustic term that propagates sound generated by volume sources to the far field. The outer limit of the hydrodynamic term will match to an outer hydrodynamic solution found later in Section 4. These solutions are now the generalized form to those presented in Tsai (1992).

3.5. *Solution for thickness-related term H_3*

H_3 is the solution arising from the interaction of the scattered sound at leading order, (3.5), with the non-uniform flow around the aerofoil nose. It satisfies

$$\begin{aligned} D(H_3) = {} & -\frac{2w^2 a\beta_\infty \sin\theta/2}{\sqrt{R}}H_0 + \frac{(\gamma+1)M_\infty^4 a\sin\theta/2}{\beta_\infty^3\sqrt{R}}\left(\frac{\partial^2 H_0}{\partial\Psi^2} + 2i\delta\frac{\partial H_0}{\partial\Phi} + (w^2 + \delta^2)H_0\right)\\ & + \frac{a(\gamma+1)M_\infty^4\sin 3\theta/2}{2\beta_\infty^3 R^{3/2}}\left(\frac{\partial H_0}{\partial\Phi} - i\delta H_0\right), \end{aligned} \tag{3.16a}$$

$$\left.\frac{\partial H_3}{\partial \Psi}\right|_{\substack{\Phi>0\\ \Psi=0}} = \frac{M_\infty^2 a H_0 \operatorname{sgn}(\Psi)}{2\beta_\infty R^{3/2}}. \tag{3.16b}$$

This is solved similarly to the H_3 term in Tsai (1992) by splitting into a particular solution, H_{3p}, and complementary solutions $H_{3c_1} + H_{3c_2} + H_{3c_3}$. Details of the solution can be found in Appendix A (including corrections to Tsai's results), along with the outer limits of the solutions;

$$H_{3p} \sim -\frac{A_n a\, \mathrm{e}^{i\pi/4} w \sin\theta\, \mathrm{e}^{iwkr}}{\sqrt{\pi}\sqrt{\delta + w}(\delta - w\cos\theta)}\left(1 - \frac{(\gamma+1)M_\infty^4}{2\beta_\infty^4 w^2}(\delta - w\cos\theta)^2\right) + L_{3p}(\theta)\frac{\mathrm{e}^{iwkr}}{\sqrt{kr}} + O(1/k), \tag{3.17}$$

and

$$H_{3c_i} \sim L_{3c_i}(\theta)\frac{\mathrm{e}^{iwkr}}{\sqrt{kr}} + O(k^{-3/2}) \quad \text{for } i = 1, 2, 3. \tag{3.18}$$

We define $L_3(\theta) = L_{3p}(\theta) + L_{3c_1}(\theta) + L_{3c_2}(\theta) + L_{3c_3}(\theta)$.

3.6. *Solution for camber-related terms $P_i, i = 1, 2, 3$*

Myers & Kerschen (1997) provide leading-edge inner solutions for a flat plate with effective angle of attack α_{eff}. Since camber and thickness are essentially independent effects in the leading-edge inner region we can immediately use their results, which yield outer limits

$$P_i(r, \theta) \sim D_i(\theta)\frac{\mathrm{e}^{ikwr}}{\sqrt{kr}}, \tag{3.19a}$$

where

$$D_1(\theta) = \frac{2iA_n\delta}{\sqrt{w}(\delta - w\cos\theta)^{3/2}}, \tag{3.19b}$$

$$D_2(\theta) = \tilde{L}_2(\theta)\ , \tag{3.19c}$$

$$D_3(\theta) = \frac{iA_n}{\sqrt{w(\delta - w\cos\theta)}}\left(1 - \frac{M_\infty^2}{\beta_\infty^2} - \frac{\delta}{\delta - w\cos\theta}\right) + \frac{iA_n(\gamma+1)M_\infty^4}{w^{3/2}\sqrt{\delta + w}\beta_\infty^4}\left(\frac{\delta}{2}\cos\theta - \frac{w}{4}\cos 2\theta\right). \tag{3.19d}$$

$\tilde{L}_2(\theta)$ is related to $L_2(\theta)$ by changing the functions (3.14) to

$$\begin{aligned} C_1' &= i2^{3/2}\left(\frac{\delta A_t^*}{\beta_\infty} - k_n A_n\right), & C_2' &= i2^{3/2}\left(\frac{k_n A_t^*}{\beta_\infty} + \delta A_n\right),\\ C_3' &= -\frac{\sqrt{2}A_t^* M_\infty^2}{\beta_\infty^3}, & C_4' &= -\frac{\sqrt{2}A_n M_\infty^2}{\beta_\infty^2}. \end{aligned} \tag{3.20}$$

4. Outer solutions

We separate the solution into four parts,

$$h = h_p + h_c + h_l + h_t.$$

Here, h_p is the particular solution due to the volume source, S. The complementary solution, h_c satisfies the boundary condition whilst $h_{l,t}$ account for the propagation of sound generated in the inner leading- and trailing-edge regions, respectively, to the far field. To leading order, h_p satisfies

$$\frac{\partial^2 h}{\partial \phi^2} + \frac{\partial^2 h}{\partial \psi^2} + k^2 w^2 h = k\varepsilon S(\phi, \psi)\, \mathrm{e}^{ik\Omega(\phi,\psi)} + O(\varepsilon). \tag{4.1}$$

Tsai (1992) and Myers (1987) obtain outer solutions $h_{p,c}$ in terms of the function, S, therefore despite our problem relying on a more general S, we can immediately take these as our outer solutions for $h_{p,c}$;

$$h_p = \frac{\varepsilon}{k} \frac{S(\phi, \psi)\, \mathrm{e}^{ik\Omega(\phi,\psi)}}{w^2 - \left(\frac{\partial \Omega}{\partial \phi}\right)^2 - \left(\frac{\partial \Omega}{\partial \psi}\right)^2} + O(\varepsilon^3), \tag{4.2}$$

$$h_c = \frac{\mathrm{sgn}(\psi)}{km(\phi)} \left(-\frac{A_n}{\beta_\infty} + 2\varepsilon \mu(\phi, 0) A_t^* + \frac{A_n M_\infty^2 \varepsilon q(\phi, 0)}{\beta_\infty} - \frac{ik_n \varepsilon S(\phi, 0)}{w^2 - \delta^2 - k_n^2} \right) \mathrm{e}^{-k|\psi| m(\phi) + ik\Omega(\phi,0)}, \tag{4.3a}$$

where

$$[m(\phi)]^2 = \left(\frac{\partial \Omega(\phi, 0)}{\partial \phi} \right)^2 - w^2(1 - 2\beta_\infty^2 \varepsilon q(\phi, 0)). \tag{4.3b}$$

Neither h_p nor h_c are acoustic waves as both convect with the mean flow, therefore all sound generated by gust-aerofoil interaction is produced in the local leading- and trailing-edge regions. The hydrodynamic particular solution, h_p matches to the leading-edge inner hydrodynamic solutions; details can be found in Myers & Kerschen (1997) and Tsai (1992). The hydrodynamic complementary solution, h_c matches to an inner trailing-edge hydrodynamic term.

4.1. *Leading and trailing-edge acoustic outer solutions*

The outer acoustic solutions are also analogous to the solutions in Myers & Kerschen (1997) and Tsai (1992) with suitably redefined terms;

$$h_l = \frac{\mathscr{D}_l(\theta)}{k^{3/2}\sqrt{r}}\, \mathrm{e}^{ikwr + ikw\varepsilon V(\theta) \int_0^r q(r', \theta)\, \mathrm{d}r' + 2ik\varepsilon F_R(-\infty)} \equiv \frac{\mathscr{D}_l(\theta)}{k^{3/2}\sqrt{r}}\, \mathrm{e}^{ikw\sigma_l(r,\theta)}, \tag{4.4}$$

where

$$\mathscr{D}_l(\theta) = L_0(\theta) + t\sqrt{k}\,(L_1(\theta) + L_2(\theta) + L_3(\theta)) + \alpha_{\mathrm{eff}}\sqrt{k}\,(D_1(\theta) + D_2(\theta) + D_3(\theta)). \tag{4.5}$$

For a uniformly-valid outer solution we must replace the non-uniformly valid term $L_{3c_2}(\theta)(kr)^{-1/2}$ within $L_3(\theta)$ by its uniformly-valid counterpart $L^u_{3c_2}(r,\theta)$.

The trailing-edge outer solution is found in trailing-edge variables, (ϕ_t, ψ_t) (with equivalent polar coordinates (r_t, θ_t)), centred on the trailing edge of the aerofoil and defined by

$$\phi = 2 \pm \frac{\Gamma}{2} + \alpha_t + \phi_t, \qquad \psi = \psi_t, \tag{4.6}$$

where Γ is the circulation around the aerofoil given by

$$\Gamma = \frac{2\pi}{\beta_\infty}\alpha_g, \tag{4.7}$$

$$\alpha_g = \alpha_i + \frac{1}{\pi}\int_0^2 \frac{\varepsilon y^{(c)}(x)}{\sqrt{x}(2-x)^{3/2}}\,\mathrm{d}x, \tag{4.8}$$

and α_t is given by $\alpha_t = \mathrm{Re}(\varepsilon F^{(t)}(2))$. The trailing-edge acoustic outer solution is given by

$$h_t = \frac{\mathscr{D}_t(\theta)}{k^2\sqrt{r_t}}\,\mathrm{e}^{ikwr_t + ikw\varepsilon V(\theta_t)\int_0^{r_t} q(r'_t,\theta_t)\,\mathrm{d}r'_t} \equiv \frac{\mathscr{D}_t(\theta_t)}{k^2\sqrt{r_t}}\,\mathrm{e}^{ikw\sigma_t(r_t,\theta_t)}. \tag{4.9}$$

$\mathscr{D}_t$ is determined by matching to the trailing-edge inner solution which follows in Section 6.1.

5. Leading-edge transition solution

The leading-edge transition solution ensures that the zero normal velocity condition holds along the entire length of the aerofoil, and not just locally at the leading edge. We suppose the total leading-edge acoustic solution is given by

$$h^u_l = h_l + h^{(t)}_{ls} + h^{(c)}_{ls}, \tag{5.1}$$

where $h^{(t,c)}_{ls}$ are the thickness- and camber-related leading-edge transition solutions that correct for the boundary condition on the surface of the aerofoil. The thickness-related solution takes the form

$$h^{(t)}_{ls}(\phi,\eta) = \frac{t}{k}\mathscr{G}(\phi,\eta)\mathrm{e}^{ikw\phi + ikw\varepsilon V(0)\int_0^r q(r',0)\,\mathrm{d}r' + 2ik\varepsilon F_R(-\infty)}, \tag{5.2}$$

where $\eta = \sqrt{k}\psi$. It must satisfy

$$2iw\frac{\partial \mathscr{G}}{\partial \phi} + \frac{\partial^2 \mathscr{G}}{\partial \eta^2} = 0, \tag{5.3}$$

and ensure that the thickness-related terms from h^u_l satisfy

$$\frac{\partial h^u_l}{\partial n} = 0 \tag{5.4}$$

along the aerofoil surface. We solve using the Laplace transform to obtain

$$\mathscr{G}(\phi,\eta)=\frac{iA_n w}{\sqrt{2w}\pi\sqrt{\delta+w}(\delta-w)}\left(1-\frac{(\gamma+1)M_\infty^4}{2\beta_\infty^4 w^2}(\delta-w)^2\right)\left(\int_0^2 \Omega(0,\xi,\xi)\frac{\mathrm{e}^{i\eta^2 w/2(\phi-\xi)}}{\sqrt{\phi-\xi}}\,\mathrm{d}\xi+\int_2^\phi \Omega(0,\xi,2)\frac{\mathrm{e}^{i\eta^2 w/2(\phi-\xi)}}{\sqrt{\phi-\xi}}\,\mathrm{d}\xi\right) \tag{5.5}$$

for $\phi>2$, where Ω is defined as

$$\Omega(\theta,\tau,\tau')=\left(\frac{a}{\tau}+\frac{\beta_\infty}{t'\tau^{3/2}}\int_0^{\tau'}\frac{\partial q^{(t)}}{\partial\theta}(r,\theta)\,\mathrm{d}r\right). \tag{5.6}$$

This yields the generalized transition solution to Tsai's result which was the specialized case of a symmetric Joukowski aerofoil.

The camber-related transition solution can be obtained directly from Myers & Kerschen (1997) since they give a solution in terms of the generalized camber distribution on the aerofoil, $\varepsilon y^{(c)}(x)$. For large ϕ this yields

$$h_{ls}^{(c)}\sim\frac{\mathrm{sgn}(\psi)\mathrm{e}^{ikw\sigma_l(\phi,0)}}{k\sqrt{r}}\frac{\mathrm{e}^{3i\pi/4}\varepsilon V(0)P_l(0\pm)}{\sqrt{2\pi w}\beta_\infty}\left[\int_0^2\frac{\mathrm{e}^{iw\eta^2/2(\phi-\xi)}(\xi y^{(c)\prime}(\xi)-y^{(c)}(\xi))}{\sqrt{\phi-\xi}\xi^{3/2}}\,\mathrm{d}\xi+2^{3/2}y^{(c)\prime}(2)\left(\frac{\mathrm{e}^{iw\eta^2/2(\phi-2)}\sqrt{\phi-2}}{\phi}-\frac{|\eta|\mathrm{e}^{-\pi i/4}\sqrt{\pi w}\mathrm{e}^{iw\eta^2/2\phi}}{\phi^{3/2}}\mathrm{erfc}[\frac{\mathrm{e}^{-\pi i/4}\sqrt{w}|\eta|}{\sqrt{\phi(\phi-2)}}]\right)\right], \tag{5.7}$$

$$\equiv\frac{1}{k}D_{ltr}(\theta)\frac{\mathrm{e}^{ikw\sigma_l(r,\theta)}}{\sqrt{r}}, \tag{5.8}$$

with

$$P_l(\theta)=\Big[L_0(\theta)+\alpha_{\mathrm{eff}}\sqrt{k}\,(D_1(\theta)+D_2(\theta)+D_3(\theta))\Big]. \tag{5.9}$$

Therefore the total far-field solution emanating from the leading edge can be written as

$$h_l^u\sim\frac{\mathrm{e}^{ikw\sigma_l(r,\theta)}}{k^{3/2}\sqrt{r}}D_l(\theta). \tag{5.10}$$

We have only given explicit results for $h_{ls}^{(t,c)}$ in the region $\phi>2$ because these are used to find the pressure jump across the wake. In the far field, except for $\theta\sim 0,2\pi$, the transition solutions are negligible.

6. Trailing-edge solutions

6.1. *Trailing-edge inner solution*

Trailing-edge inner coordinates are defined as $(\Phi_t, \Psi_t) = k(\phi_t, \psi_t)$ and the inner potential is given by $H_t(\Phi_t, \Psi_t)$. Upon substituting the inner trailing-edge coordinates into (2.9a) we obtain

$$\frac{\partial^2 H_t}{\partial \Phi_t^2} + \frac{\partial^2 H_t}{\partial \Psi_t^2} + w^2 H_t = O(\frac{\varepsilon}{k}). \tag{6.1}$$

The source term is negligible in the trailing-edge region since there is a lesser effect of curvature at the trailing edge than at the leading edge, resulting in a different scaling for q at the trailing edge, $q = O(1)$. Hence H_t satisfies the homogeneous Helmholtz equation subject to boundary condition

$$\left.\frac{\partial H_t}{\partial \Psi_t}\right|_{\substack{\Phi_t<0\\ \Psi_t=0}} = -\frac{A_n}{k\beta_\infty}\, \mathrm{e}^{i\delta\Phi_t + ik\delta(2\pm\Gamma/2+\alpha_t)+ik\varepsilon g(\phi,0)}. \tag{6.2}$$

Pressure and normal velocity must be continuous across the wake of the aerofoil, $\Psi_t = 0, \Phi_t > 0$.

Myers (1987) gives a solution satisfying the Helmholtz equation and normal velocity condition;

$$H_t^h = \frac{\mathrm{sgn}(\Psi_t)A_n}{\beta_\infty\sqrt{\delta^2 - w^2}}\, \mathrm{e}^{ik\delta(2\pm\Gamma/2+\alpha_t)+ik\varepsilon g(2,0\pm)}\, \mathrm{e}^{-|\Psi_t|\sqrt{\delta^2-w^2}}\, \mathrm{e}^{i\delta\Phi_t}. \tag{6.3}$$

This is a hydrodynamic solution with outer limit matching onto the hydrodynamic complementary solution, h_c mentioned in Section 4.

We now require a local inner acoustic solution, H_t^a, to correct the discontinuous pressure fluctuations across the wake due to the leading-edge acoustic field. The total inner trailing-edge solution is then given by $H_t = H_t^h + H_t^a$. Recall the non-dimensionalized modified pressure at the trailing edge due to the leading-edge ray field is given by

$$p_l = ik(\delta - w\cos\theta)h_l^u(r,\theta)\, \mathrm{e}^{-ik\delta M_\infty^2\phi}. \tag{6.4}$$

The pressure jump caused by the leading-edge field across the wake is given in Appendix B, where we define $\Delta p(\phi_t)$.

The boundary conditions for the inner acoustic trailing-edge problem are then as follows;

$$\mathrm{e}^{-iC_+}\left.\frac{\partial H_t^a}{\partial \Psi_t}\right|_{\substack{\Phi_t>0\\ \Psi_t=0+}} = \mathrm{e}^{-iC_-}\left.\frac{\partial H_t^a}{\partial \Psi_t}\right|_{\substack{\Phi_t>0\\ \Psi_t=0-}} \tag{6.5a}$$

imposes continuity of displacement across the wake, where the constants $C_\pm$ are defined by

$$C_\pm = k\delta M_\infty^2(2 \pm \Gamma/2 + \alpha_t), \tag{6.5b}$$

and the continuity of pressure across the wake requires

$$\mathrm{e}^{-iC_-}\left[\frac{\partial H_t^a}{\partial \Phi_t} - i\delta H_t^a\right]_{\substack{\Phi_t>0\\ \Psi_t=0-}} - \mathrm{e}^{-iC_+}\left[\frac{\partial H_t^a}{\partial \Phi_t} - i\delta H_t^a\right]_{\substack{\Phi_t>0\\ \Psi_t=0+}} = \frac{\Delta p(0)}{\sqrt{k}}\, \mathrm{e}^{iw\Phi_t}. \tag{6.5c}$$

Since the hydrodynamic solution enforces zero normal velocity on the aerofoil surface we impose

$$\left.\frac{\partial H_t^a}{\partial \Psi_t}\right|_{\substack{\Phi_t<0\\ \Psi_t=0}} = 0. \tag{6.5d}$$

By ensuring that our new trailing-edge problem is now of the same form as the trailing-edge problems in Myers & Kerschen (1997) and Tsai (1992), but with a new definition for Δp, we can immediately write down the inner solution as

$$H_t^a = \frac{\operatorname{sgn}(\Psi_t) i\sqrt{2w}\Delta p(0)\, \mathrm{e}^{iC\pm}}{4\pi k^{3/2}} \int_{-\infty}^{\infty} \frac{\mathrm{e}^{-i\lambda\Phi_t - |\Psi_t|\sqrt{\lambda^2-w^2}}}{(\lambda+\delta)(\lambda+w)\sqrt{\lambda-w}}\,\mathrm{d}\lambda. \tag{6.6}$$

This has outer limit

$$H_t^a \sim T(\theta_t)\frac{\mathrm{e}^{ikwr_t}}{k^2\sqrt{r_t}}, \tag{6.7a}$$

where

$$T(\theta_t) = -\frac{\mathrm{e}^{i\pi/4+iC\pm}\Delta p(0)\operatorname{sgn}(\psi_t)}{2\sqrt{\pi w(1-\cos\theta_t)}(\delta - w\cos\theta_t)}. \tag{6.7b}$$

The uniformly-valid outer limit of H_t^a is obtained by replacing T with

$$T^u(r_t,\theta_t) = \frac{\operatorname{sgn}(\psi_t)\, i\Delta p(0)\, \mathrm{e}^{iC\pm}}{2(\delta-w)}\left[\operatorname{erfc}(\mathrm{e}^{-i\pi/4}\sqrt{w(1-\cos\theta_t)kr_t})\,\mathrm{e}^{ikwr_t(\cos\theta_t-1)}\sqrt{kr_t}\right.$$
$$\left. - \frac{\sqrt{2w}\,\mathrm{e}^{i\pi/4}|\sin\theta_t/2|}{\sqrt{\pi}(\delta - w\cos\theta_t)}\right]. \tag{6.7c}$$

This trailing-edge inner solution matches the trailing-edge outer acoustic solution, (4.9), if $\mathscr{D}_t(\theta_t) = T(\theta_t)$.

6.2. *Trailing-edge transition solution*

Despite our trailing-edge inner solution containing arbitrary terms, q and F (within Δp) to allow for an aerofoil of arbitrary shape with a parabolic leading edge, we have been able to construct a solution that is of the same form as the solution found by Tsai (1992) by appropriately redefining the pressure jump function, Δp. This allows us to use the transition solutions derived by Myers & Kerschen (1997) and Tsai (1992) here (with suitably redefined terms such as Δp, which we can write as $\Delta p^{(t)} + \Delta p^{(c)}$ to separate out the thickness-related and camber-related terms), and also immediately tells us that we have a matching between the trailing-edge transition and inner solutions.

7. Total far-field solution

The total contribution to the acoustics due to trailing-edge solutions, h_t^u, is obtained by summing the trailing-edge outer solution with the trailing-edge transition solution and subtracting any common terms. It is given in full in Appendix C. We write the trailing-edge solution as

$$h_t^u \sim \frac{D_t(\theta_t)}{k^2\sqrt{r_t}}\,\mathrm{e}^{ikw\sigma_t(r_t,\theta_t)}. \tag{7.1}$$

The total far-field solution, h, is obtained by summing the contributions from the leading- and trailing-edge fields, giving

$$h = \frac{\mathrm{e}^{ikw\sigma_l}}{k^{3/2}\sqrt{r}}\left[D_l(\theta) + D_t(\theta)\frac{\mathrm{e}^{ikw\sigma_s}}{\sqrt{k}}\right], \tag{7.2}$$

where σ_s is the phase shift between the leading- and trailing-edge ray fields, and $D_{l,t}(\theta)$ are the far-field potential directivities for the leading and trailing edges. The phase shift, σ_s, is given by

$$\sigma_s^{\pm} = \sigma_t - \sigma_l = \frac{V(\theta)}{\beta_\infty}\left(2\alpha_i \sin\theta + \cos\theta(\pm\alpha_g\pi + \beta_\infty\alpha_t)\right) + (2 \pm \frac{\alpha_g\pi}{\beta_\infty} + \alpha_t)\cos\theta - 2\varepsilon F_R(-\infty). \tag{7.3}$$

The $\pm$ denotes the phase shift above and below the aerofoil, respectively, and is present due to the non-zero mean circulation.

8. Results

We first must convert our solution, (7.2), from potential-streamline coordinates, (r,θ), to physical coordinates, (r_p,θ_p), so that we produce results for physical parameters. The relationship, in the far field, between physical and potential-streamline coordinates is given by

$$r = (1 - M_\infty^2 \sin\theta)^{1/2} r_p + O(t, \alpha_{\text{eff}}), \tag{8.1a}$$

$$\cos\theta = \frac{\beta_\infty \cos\theta_p}{\sqrt{1 - M_\infty^2\cos^2\theta_p}}. \tag{8.1b}$$

8.1. *Far-field pressure directivity*

Initially we focus on the directivity, $|D(\theta)|$, of the far-field pressure which, by using (2.11), relates to h via

$$D(\theta) = ik(\delta - w\cos\theta)h(r,\theta)\,\mathrm{e}^{-ik\delta M_\infty^2\phi}. \tag{8.2}$$

The individual effects of varying angle of attack, camber and thickness on the far-field directivity have previously been discussed in detail in Myers & Kerschen (1995, 1997) and Tsai (1992), respectively, therefore the main aim of this article is to present a solution that assesses the combined effects of camber and thickness, fully extending these previous works.

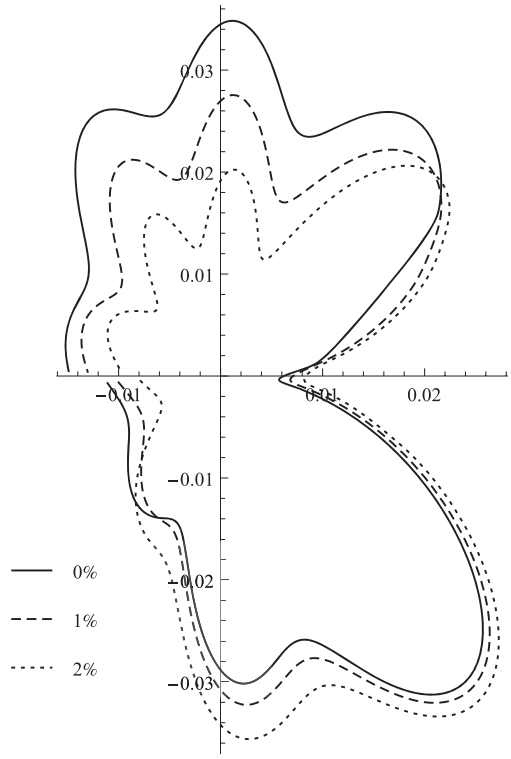

Fig. 3. Far-field scattered pressure directivity for a 10% thick Joukowski aerofoil with $k = 5$, $\alpha_i = 0°$, $M_\infty = 0.6$, $k_3 = 0$ and $\theta_g = 45°$. Maximum camber is varied from 0 to 2%, and the location of maximum camber is at 10% chord length.

Figures 3 and 4 illustrate that our generalized solution is in agreement with the previous solutions by Tsai (1992)[1] and Myers & Kerschen (1997) in the limits of zero camber and thickness, respectively. We define $\theta_g = \arctan(\beta_\infty k_n/k_t)$ as the gust angle with respect to the uniform flow direction. Figure 3 illustrates the effects of increasing the camber angle of a thick aerofoil, with the solid line agreeing with the dotted line in Fig. 4.28 from Tsai (1992). Above the aerofoil, the far-field noise is decreased with increasing camber, whilst below there is a small increase in far-field noise which is the result observed in Myers & Kerschen (1997) for zero-thickness aerofoils. Figure 4 illustrates the effect of increasing thickness for a cambered aerofoil, with the solid line agreeing with Fig. 4 from Myers & Kerschen (1997); we see a decrease in far-field noise as thickness increases at almost all observer angles, which is a known result for symmetric (i.e. uncambered) aerofoils (Gill *et al.*, 2013).

It is not sufficient however to simply increase both camber and thickness to reduce the total noise, as illustrated by Fig. 5, where we see increasing both camber and thickness does not lead to a decrease in far-field noise; notice in particular the second quadrant, in which increasing thickness or camber independently showed a noise decrease, now simultaneously does not exhibit the same behaviour. This indicates that the mechanisms for noise reduction by increasing thickness or increasing camber are

[1] There are only minor differences between the result here and in Tsai (1992) due to the corrections to various leading-edge inner terms.

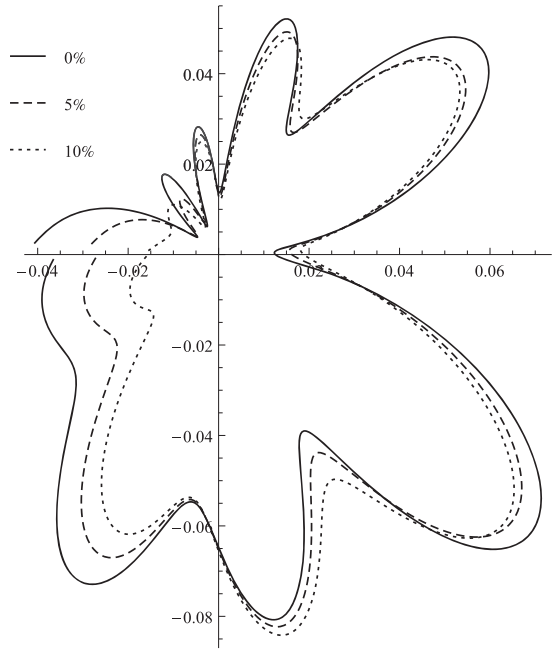

Fig. 4. Far-field scattered pressure directivity for a 6-33 cambered aerofoil (as defined in Myers & Kerschen, 1997) with $k = 8$, $\alpha_i = 0°$, $M_\infty = 0.5$, $k_3 = 0$ and $\theta_g = 60°$. Thickness is varied from 0 to 10%.

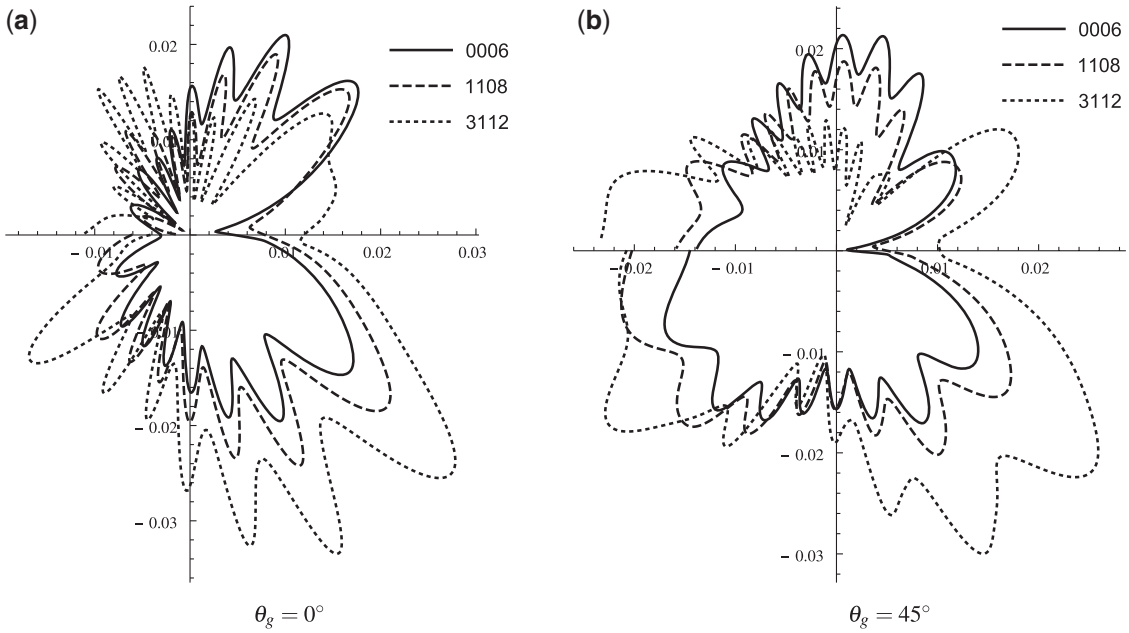

$\theta_g = 0°$ $\theta_g = 45°$

Fig. 5. Far-field scattered pressure directivity for NACA 4-digit series aerofoils with $M_\infty = 0.7$, $\alpha_i = 0$ and $k = 8$. (a) $\theta_g = 0°$. (b) $\theta_g = 45°$.

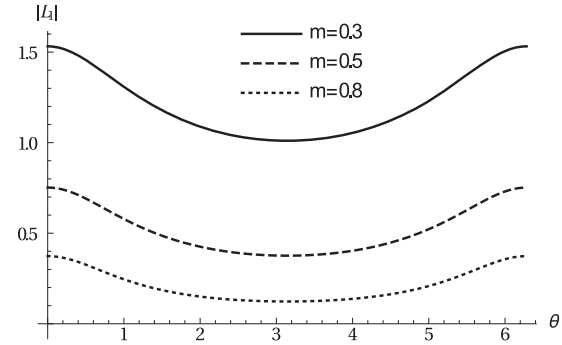

Fig. 6. Magnitude of $L_1(\theta)$ for various leading-edge geometries, $y \sim 2a\varepsilon t' x^m$, for $k = 10$, $t = 0.06$, $\theta_g = 45°$, $M_\infty = 0.6$.

different, and therefore can interfere with one another in such a way that the noise is in fact increased in certain cases. This interference of camber and thickness terms can be seen directly from the mathematics; whilst thickness and camber terms are additively separated for amplitude terms (e.g. in (3.3)), the phase shift, (7.3), between the leading- and trailing-edge ray fields contains both thickness and camber terms and therefore influences both the thickness and camber amplitude terms.

The discontinuity in pressure along $\theta = \pi$ is a feature to some extent of all results and is due to the scattered field from the trailing edge interacting with the leading edge. If we went to a higher order still in our analysis then we would remove this discontinuity with an additional leading-edge solution, in much the same way that we removed the discontinuity at the trailing edge.

8.2. *Effect of leading-edge radius*

In Section 3.3 we explicitly calculated the first thickness-related correction term, L_1 in the case of an arbitrary leading-edge geometry, $y \sim 2a\varepsilon t' x^m$. For constant camber aerofoils we see in Fig. 4 the effect of increasing thickness is to decrease the total far-field noise for almost all observer angles, therefore the effect of the (far-field) leading-edge terms, $L_{1,2,3}$ are to subtract from the flat-plate term L_0. As the leading-edge radius decreases, $m \to 1$ the size of the correction factor, εk^{1-m} decreases resulting in a smaller term subtracted from L_0, and we expect therefore that a thinner leading edge will generate more noise than a wider leading edge, which is indeed the result obtained through experimental measurements (Chaitanya *et al.*, 2015).

In Fig. 6 we plot the magnitude of the leading-edge term $\varepsilon k^{1-m} L_1(\theta)$ for various leading-edge geometries and indeed see for all values of θ, a larger value of m results in a smaller leading-edge term. In Fig. 7 we plot the magnitude of all leading-edge terms, $L_{1,2,3}(\theta)$ in the case of a parabolic leading edge and see that L_1 is typical of the magnitude of all of the thickness-related leading-edge correction factors, therefore we would expect similar reductions for $\varepsilon k^{1-m} L_{2,3}$ as m increases as we have seen in Fig. 6 for $\varepsilon k^{1-m} L_1$.

9. Conclusions

In this article we have obtained an analytic solution for the sound generated by high-frequency gust-aerofoil interaction, correct to two orders of magnitude in the amplitude and phase. This has significantly extended the previous work by Myers & Kerschen (1997) and Tsai (1992) who found analytic solutions

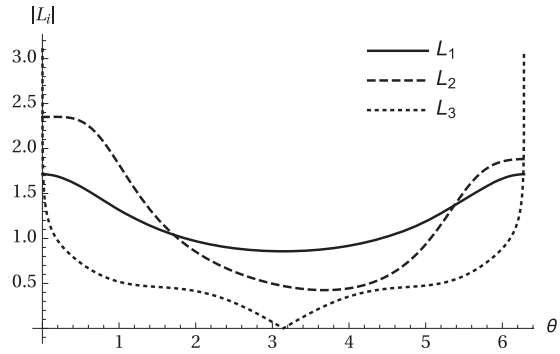

Fig. 7. Magnitude of thickness-related leading-edge terms, $L_{1,2,3}(\theta)$ for a parabolic leading edge, $m = 0.5$, for $k = 10$, $t = 0.06$, $\theta_g = 45°$, $M_\infty = 0.6$.

in the cases of zero-thickness and zero-camber, respectively. Turbulence is commonly decomposed into a Fourier series of gust components, and each Fourier frequency is considered individually; it is therefore important to be able to access acoustic solutions at high frequencies in order to accurately describe the noise generated by an aerofoil interacting with turbulence in a uniform steady flow. Since numerical schemes commonly struggle at high frequencies ($k \gtrsim 5$), this work will allow acoustic solutions to be found at a wider range of frequencies than are currently available; computational codes can implement the far-field approximations as boundary conditions rather than imposing non-reflective boundary conditions, which are increasingly difficult to resolve for a given aerofoil and background flow as the frequency of the initial gust increases.

It is known that increasing thickness or camber can reduce far-field noise generated by gust-aerofoil interaction, but these results are obtained only in the cases of constant (usually zero) camber and thickness. We have found that, due to different mechanisms allowing for the reduction of noise, interference between thickness- and camber-related effects can in fact lead to a noise increase in the far field. Therefore, if one wishes to alter the geometry of an aerofoil to reduce noise, it is not sufficient to simply increase both thickness and camber.

We have also investigated the effects of leading-edge geometry on the noise generated by gust-aerofoil interaction and found, in agreement with experimental results, that an increased leading-edge radius can decrease generated noise for the case of fixed camber. Further study is required to understand the combined effect of varying both leading-edge radius and camber.

Acknowledgements

My original submission to the Lighthill-Thwaites Prize was based upon gust-aerofoil interaction in steady shear flow (Ayton & Peake, 2015). Some of this work, in steady uniform flow, along with the submitted work, form part of my Ph.D thesis, (Ayton, 2014).

Funding

EPSRC (EP/I010440/1) to L.J.A.

References

Ayton, L. J. (2014) Asymptotic approximations for the sound generated by aerofoils in unsteady subsonic flows. *Ph.D. Thesis*, University of Cambridge, Cambridge, UK.

Ayton, L. J. & Peake, N. (2013) On high-frequency noise scattering by aerofoils in flow. *J. Fluid Mech.,* **734**, 144–182.

Ayton, L. J. & Peake, N. (2015) On high-frequency sound generated by gust-aerofoil interaction in shear flow. *J. Fluid Mech.,* **766**, 297–325.

Chaitanya, P., Gill, J., Narayanan, P., Joseph, P., Vanderwel, C., Zhang, X. & Ganapathisubramani, B. (2015) Aerofoil geometry effects on turbulence interaction noise. *21st AIAA/CEAS Aeroacoustics Conference, Dallas, TX*, 2015–2830.

Gill, J., Zhang, X., Joseph, P. F. & Node-Langlois, T. (2013) Effects of real airfoil geometry on leading edge gust interaction noise. *19th AIAA/CEAS Aeroacoustics Conference, Berlin, DE*, 2013–2203.

Goldstein, M. E. (1978) Unsteady vortical and entropic distortions of potential flows round arbitrary obstacles. *J. Fluid Mech.,* **89**, 433–468.

Hixon, R., Scott, J. R., Sawyer, S. & Nallasamy, M. (2006) Application of a nonlinear computational aeroacoustics code to the gust-airfoil problem. *AIAA J.,* **44**, 323–328.

Hunt, J. C. R. (1973) A theory of turbulent flow round two-dimensional bluff bodies. *J. Fluid Mech.,* **61**, 625–706.

Kerschen, E. J. & Balsa, T. F. (1981) Transformation of the equation governing disturbances of a two-dimensional compressible flow. *AIAA J.,* **19**, 1367–1370.

Kerschen, E. J. & Myers, M. R. (1987) Perfect gas effects in compressible rapid distortion theory. *AIAA J.,* **25**, 504–507.

Myers, M. R. (1987) Effect of airfoil mean loading on high-frequency gust interaction noise. *Ph.D. Thesis*, University of Arizona, Arizona, US.

Myers, M. R. & Kerschen, E. J. (1995) Influence of incidence angle on sound generation by airfoils interacting with high-frequency gusts. *J. Fluid Mech.,* **292**, 271–304.

Myers, M. R. & Kerschen, E. J. (1997) Influence of camber on sound generation by airfoils interacting with high-frequency gusts. *J. Fluid Mech.,* **353**, 221–259.

Thwaites, B. (1960) *Incompressible Aerodynamics: An Account of the Theory and Observation of the Steady Flow of Incompressible Fluid Past Aerofoils, Wings, and Other Bodies*. New York: Dover Publications.

Tsai, C-T. (1992) Effect of airfoil thickness on high-frequency gust interaction noise. *Ph.D. Thesis*, University of Arizona, Arizona, US.

Van der Waerden, B. L. (1952) On the method of saddle points. *Appl. Sci. Res. Sect. B,* **2**, 33–45.

Van Dyke, M. (1975) *Perturbation Methods in Fluid Mechanics*. Stanford, California: Parabolic Press.

Appendix A. Leading-edge inner solution

The analysis for the leading-edge inner term, H_3, is given here. It follows the procedure set out by Tsai (1992) however includes corrections to his stated results. We choose a particular solution to (3.16) of the form

$$H^*_{3p} = \frac{A_n w^2 a\,\mathrm{sgn}(\Psi)\sqrt{R}}{\pi\sqrt{\delta + w}}\left(\cos\theta/2\int_{-\infty}^{\infty} C_1(\lambda)\,\mathrm{e}^{a(\lambda,\Phi,\Psi)}\,\mathrm{d}\lambda + \sin\theta/2\int_{-\infty}^{\infty} C_2(\lambda)\,\mathrm{e}^{a(\lambda,\Phi,\Psi)}\,\mathrm{d}\lambda \right.$$
$$\left. + \frac{\cos\theta/2}{R}\int_{-\infty}^{\infty} C_3(\lambda)\,\mathrm{e}^{a(\lambda,\Phi,\Psi)}\,\mathrm{d}\lambda + \frac{\sin\theta/2}{R}\int_{-\infty}^{\infty} C_4(\lambda)\,\mathrm{e}^{a(\lambda,\Phi,\Psi)}\,\mathrm{d}\lambda\right). \quad \text{(A.1a)}$$

Applying the Helmholtz operator and solving for $C_{1,2,3,4}(\lambda)$ yields

$$H^*_{3p} = \frac{A_n a}{\pi\sqrt{\delta+w}}\left(\sqrt{R}\cos\theta/2\int_{-\infty}^{\infty}\sqrt{\lambda-w}(\lambda+\delta)\left[\frac{1}{(\lambda+\delta)^2}-\frac{(\gamma+1)M_\infty^4}{2\beta_\infty^4 w^2}\right]\mathrm{e}^{a(\lambda,\Phi,\Psi)}\,\mathrm{d}\lambda\right.$$
$$-i\,\mathrm{sgn}(\Psi)\sqrt{R}\sin\theta/2\int_{-\infty}^{\infty}\frac{\lambda(\lambda+\delta)}{\sqrt{\lambda+w}}\left[\frac{1}{(\lambda+\delta)^2}-\frac{(\gamma+1)M_\infty^4}{2\beta_\infty^4 w^2}\right]\mathrm{e}^{a(\lambda,\Phi,\Psi)}\,\mathrm{d}\lambda$$
$$-\frac{(\gamma+1)M_\infty^4}{4\beta_\infty^4 w^2}\frac{i\cos\theta/2}{\sqrt{R}}\int_{-\infty}^{\infty}\sqrt{\lambda-w}\,\mathrm{e}^{a(\lambda,\Phi,\Psi)}\,\mathrm{d}\lambda$$
$$\left.+\mathrm{sgn}(\Psi)\frac{(\gamma+1)M_\infty^4}{4\beta_\infty^4 w^2}\frac{\sin\theta/2}{\sqrt{R}}\int_{-\infty}^{\infty}\frac{\lambda}{\sqrt{\lambda+w}}\,\mathrm{e}^{a(\lambda,\Phi,\Psi)}\,\mathrm{d}\lambda\right). \tag{A.1b}$$

To evaluate this behaviour at small R we must consider both local and global contributions from each integral. Full details can be found in Ayton (2014). By doing so, we find the asymptotic behaviour of H^*_{3p} for $R \ll 1$ to be

$$H^*_{3p} \sim \frac{A_n a\,\mathrm{e}^{i\pi/4}(\gamma+1)M_\infty^4}{2\sqrt{\pi}\beta_\infty^4 w^2\sqrt{\delta+w}}\left(\frac{\sin 2\theta}{R^2}+\frac{i\delta\sin\theta}{R}\right), \tag{A.2}$$

which differs from the result in Tsai (1992). We see (A.2) is singular at $R=0$, which is not permitted (Tsai, 1992), hence we need a complementary solution to eliminate the singularities. The appropriate solution comprises of Hankel functions of the first kind or orders 1 and 2; $H^{(1)}_{1,2}(wR)$,

$$H_{3p} = H^*_{3p} + \frac{A_n a\,\mathrm{e}^{i\pi/4}(\gamma+1)M_\infty^4}{2\sqrt{\pi}\beta_\infty^4 w^2\sqrt{\delta+w}}\left(-\frac{\pi w^2 i}{4}H_2^{(1)}(wR)\sin 2\theta+\frac{\pi\delta w}{2}H_1^{(1)}(wR)\sin\theta\right) \tag{A.3}$$

Finally, we require a complementary solution, H_{3c}, that satisfies the boundary condition on the aerofoil, i.e.

$$D(H_{3c}) = 0, \tag{A.4a}$$

$$\left.\frac{\partial H_{3c}}{\partial\Psi}\right|_{\substack{\Phi>0\\ \Psi=0}} = d(\Phi), \tag{A.4b}$$

where

$$d(\Phi) = -\frac{A_n M_\infty^2 a}{4\pi\beta_\infty^2\sqrt{\delta+w}}\frac{1}{\Phi^{3/2}}\int_{-\infty}^{\infty}\frac{\mathrm{e}^{-i\lambda\Phi}}{(\lambda+\delta)\sqrt{\lambda+w}}\,\mathrm{d}\lambda-\left.\frac{\partial H^*_{3p}}{\partial\Psi}\right|_{\substack{\Phi>0\\ \Psi=0}}. \tag{A.4c}$$

We solve (A.4) using the Wiener–Hopf method. To simplify, we set

$$d(\Phi) = d_1(\Phi)+d_2(\Phi)+d_3(\Phi),$$

where

$$d_1(\Phi) = -\frac{A_n a}{\sqrt{\delta^2-w^2}}\,\mathrm{e}^{i\delta\Phi}\left(2(\delta^2-w^2)\sqrt{\Phi}-\frac{i\delta}{\sqrt{\Phi}}\right), \tag{A.5a}$$

$$d_2(\Phi) = \frac{A_n a w\, \mathrm{e}^{iw\Phi + i\pi/4}}{\sqrt{\pi}\sqrt{\delta + w}(\delta - w)} \left(1 - \frac{(\gamma+1)M_\infty^4}{2\beta_\infty^4 w^2}(\delta - w)^2\right) \frac{1}{\Phi}, \tag{A.5b}$$

$$\begin{aligned} d_3(\Phi) =& \frac{A_n a\, \mathrm{e}^{iw\Phi + i\pi/4}}{\sqrt{\pi}\sqrt{\delta + w}} \left[2i(\delta + w) - \frac{w}{(\delta - w)\Phi} - \frac{(\gamma+1)M_\infty^4}{2\beta_\infty^4 w^2} \left(\frac{2}{\Phi^3} + \frac{i(\delta - 2w)}{\Phi^2} \right) \right. \\ &+ \frac{\sqrt{\pi}\mathrm{e}^{i(\delta - w)\Phi - i\pi/4}}{\sqrt{\delta - w}} \left(2(\delta^2 - w^2)\sqrt{\Phi} - \frac{i\delta}{\sqrt{\Phi}} \right) \operatorname{erfc}(\mathrm{e}^{i\pi/4}\sqrt{(\delta - w)\Phi}) \\ &+ \frac{(\gamma+1)M_\infty^4}{4\beta_\infty^4 w^2} \pi w\, \mathrm{e}^{-iw\Phi} \left(\frac{iw}{\Phi} H_2^{(1)}(w\Phi) - \frac{\delta}{\Phi} H_1^{(1)}(w\Phi) \right) \\ &\left. + \frac{A_n a M_\infty^2\, \mathrm{e}^{i\delta\Phi}}{\beta_\infty^2 \sqrt{\delta^2 - w^2}\Phi^{3/2}} \operatorname{erf}(\mathrm{e}^{i\pi/4}\sqrt{(\delta - w)\Phi}) \right], \end{aligned} \tag{A.5c}$$

and define

$$H_{3c} = \Sigma_{j=1}^3 H_{3c_j}, \tag{A.6}$$

where H_{3c_i} corresponds to boundary condition d_i.

Using the Wiener–Hopf method to obtain integral form solutions for the H_{3c_i} then the method of steepest descents, we obtain outer limits of our inner solutions;

$$H_{3p} \sim -\frac{A_n a\, \mathrm{e}^{i\pi/4} w \sin\theta\, \mathrm{e}^{iwkr}}{\sqrt{\pi}\sqrt{\delta + w}(\delta - w\cos\theta)} \left(1 - \frac{(\gamma+1)M_\infty^4}{2\beta_\infty^4 w^2}(\delta - w\cos\theta)^2\right) + L_{3p}(\theta)\frac{\mathrm{e}^{iwkr}}{\sqrt{kr}} + O(1/k), \tag{A.7}$$

where

$$L_{3p}(\theta) = \frac{iA_n a\sqrt{w}(\gamma+1)M_\infty^4}{2\sqrt{2}\beta_\infty^4 w^2\sqrt{\delta + w}} \left(\frac{w}{2}\sin 2\theta - \delta\sin\theta\right), \tag{A.8}$$

and

$$H_{3c_i} \sim L_{3c_i}(\theta)\frac{\mathrm{e}^{iwkr}}{\sqrt{kr}} + O(k^{-3/2}) \quad \text{for } i = 1, 2, 3, \tag{A.9a}$$

where

$$\begin{aligned} L_{3c_1}(\theta) = \frac{A_n a\sqrt{w}\,\operatorname{sgn}(\Psi)\cos(\theta/2)}{\sqrt{2}\sqrt{\delta^2 - w^2}(\delta - w\cos\theta)} \left[\frac{w - \delta\cos\theta}{\sqrt{\delta - w\cos\theta}} \left(1 - \frac{2}{\pi}\arcsin\left[\frac{\sqrt{w(1+\cos\theta)}}{\sqrt{w + \delta}} \right] \right) \right. \\ \left. - \frac{2}{\pi}(\delta - w)\sqrt{(1 + \cos\theta)} \right], \end{aligned} \tag{A.9b}$$

$$L_{3c_2}(\theta) = -\frac{\sqrt{2}i\,\operatorname{sgn}(\psi)A_n a\sqrt{w}}{\pi\sqrt{\delta + w}(\delta - w)} \left(1 - \frac{(\gamma+1)M_\infty^4}{2\beta_\infty^4 w^2}(\delta - w)^2\right) \log\left[\frac{\sqrt{2} + \sqrt{1 + \cos\theta}}{\sqrt{1 - \cos\theta}} \right], \tag{A.9c}$$

$$L_{3c_3}(\theta) = -\frac{\operatorname{sgn}(\psi)\,\mathrm{e}^{i\pi/4}}{\sqrt{2\pi w}} \int_0^\infty \mathrm{e}^{-iw\cos\theta x}\operatorname{erf}(\mathrm{e}^{-i\pi/4}\sqrt{w(1+\cos\theta)x})d_3(x)\,\mathrm{d}x. \tag{A.9d}$$

The expressions for L_{3c_1}, L_{3c_2} vary from those presented in Tsai (1992). L_{3c_2} is singular as $\theta \to 0, \pi$, however a uniformly valid expression can be obtained by using Van der Waerden's method (Van der Waerden, 1952), rather than steepest descents;

$$\begin{aligned} L^u_{3c_2}(r,\theta) = &-\frac{\sqrt{2}\operatorname{sgn}(\psi)A_n a i\sqrt{w}}{\pi\sqrt{\delta+w}(\delta-w)}\left(1-\frac{(\gamma+1)M_\infty^4}{2\beta_\infty^4 w^2}(\delta-w)^2\right) \\ &\left[\frac{\sqrt{2}}{\sqrt{\pi}\sqrt{1+\cos\theta}}\left(\frac{\sqrt{\pi}}{2}\log(kr) - \int_{-\infty}^{\infty}\log(s+\mathrm{e}^{i\pi/4}\sqrt{w(1-\cos\theta)kr})\,\mathrm{e}^{-s^2}\,\mathrm{d}s\right)\right. \\ &\left. + \log\left(\frac{\sqrt{2}+\sqrt{1+\cos\theta}}{\sqrt{1-\cos\theta}}\right) + \frac{\log(1-\cos\theta)}{\sqrt{2}\sqrt{1+\cos\theta}} + \frac{i\pi+2\log(w)}{2\sqrt{2}\sqrt{1+\cos\theta}}\right]. \end{aligned} \tag{A.9e}$$

Appendix B. Pressure jump

The pressure jump across the trailing edge is given by

$$\begin{aligned} p_l|_{\psi=0+} - p_l|_{\psi=0-} = &\frac{i(\delta-w)}{\sqrt{k}\sqrt{2+\phi_t}}\,\mathrm{e}^{ik(w-\delta M_\infty^2)(2+\phi_t+\alpha_t)+ikw\varepsilon V(0)\int_0^\phi q(r',0)\,\mathrm{d}r'+2ik\varepsilon F_R(-\infty)} \\ &\left[\mathrm{e}^{ik(w-\delta M_\infty^2)\Gamma/2}\left\{P_l(0)+t\sqrt{k}[L_1(0)+L_2(0)+L_{3p}(0)+L_{3c_1}(0)+L_{3c_2}(0)\right.\right. \\ &+L_{3c_3}(0)]+t\sqrt{k}\frac{iA_n\sqrt{w}}{\sqrt{2}\pi\sqrt{\delta+w}(\delta-w)}\left(1-\frac{(\gamma+1)M_\infty^4}{2\beta_\infty^4 w^2}(\delta-w)^2\right) \\ &\left\{\int_0^2 \Omega(0,\xi,\xi)\frac{\sqrt{2+\phi_t}}{\sqrt{2+\phi_t-\xi}}\,\mathrm{d}\xi + \int_2^{2+\phi_t}\Omega(0,\xi,2)\frac{\sqrt{2+\phi_t}}{\sqrt{2+\phi_t-\xi}}\,\mathrm{d}\xi\right. \\ &\left.\left.\left.-\frac{a}{2}\left(\log[32k(\phi_t+2)w]+\tilde{\gamma}-\frac{\pi i}{2}\right)\right\}\right]\right\} \\ &-\left[\mathrm{e}^{-ik(w-\delta M_\infty^2)\Gamma/2}\left\{P_l(2\pi)+t\sqrt{k}[L_1(2\pi)+L_2(2\pi)+L_{3p}(2\pi)+L_{3c_1}(2\pi)+L_{3c_2}(2\pi)\right.\right. \\ &+L_{3c_3}(2\pi)]-t\sqrt{k}\frac{iA_n\sqrt{w}}{\sqrt{2}\pi\sqrt{\delta+w}(\delta-w)}\left(1-\frac{(\gamma+1)M_\infty^4}{2\beta_\infty^4 w^2}(\delta-w)^2\right) \\ &\left\{\int_0^2 \Omega(0,\xi,\xi)\frac{\sqrt{2+\phi_t}}{\sqrt{2+\phi_t-\xi}}\,\mathrm{d}\xi + \int_2^{2+\phi_t}\Omega(0,\xi,2)\frac{\sqrt{2+\phi_t}}{\sqrt{2+\phi_t-\xi}}\,\mathrm{d}\xi\right. \\ &\left.\left.\left.-\frac{a}{2}\left(\log[32k(\phi_t+2)w]+\tilde{\gamma}-\frac{\pi i}{2}\right)\right\}\right]\right\} + \sqrt{k}\frac{\mathrm{e}^{\pi i/4}i\varepsilon V(0)}{\sqrt{\pi w}\beta_\infty} \\ &\times\int_0^2\frac{\xi y^{(c)\prime}(\xi)-y^{(c)}(\xi)}{\sqrt{2-\xi}\xi^{3/2}}\,\mathrm{d}\xi\left(\mathrm{e}^{ik(w-\delta M_\infty^2)\Gamma/2}P_l(0)+\mathrm{e}^{-ik(w-\delta M_\infty^2)\Gamma/2}P_l(2\pi)\right)\Bigg], \end{aligned} \tag{B.1}$$

which we write as

$$p_l|_{\psi=0+} - p_l|_{\psi=0-} = \frac{\Delta p(\phi_t)}{\sqrt{k}}\,\mathrm{e}^{ik(w-\delta M_\infty^2)\phi_t}\,\mathrm{e}^{ikw\varepsilon V(0)[\int_0^\phi q\,\mathrm{d}r - \int_0^2 q\,\mathrm{d}r]}. \tag{B.2}$$

Appendix C. Trailing-edge solution

The total acoustic field emanating from the trailing edge of the aerofoil, h_t^u, is given by summing the trailing-edge outer solution with the transition solution and subtracting any common terms;

$$\begin{aligned}
h_t^u(r_t,\theta_t) \sim\ & \\
& \frac{\mathrm{e}^{iC_\pm}\,\mathrm{e}^{ikw\sigma_t(r_t,\theta_t)}}{\sqrt{2}\sqrt{r_t}k^2(\delta - w\cos\theta_t)}\Bigg\{-\mathrm{sgn}(\psi_t)i(P_+ - P_-)E(k,\theta_t) \\
& - \frac{2\sqrt{k}wV(0)(\alpha_i - \varepsilon y^{(c)\prime}(2))(P_+ - P_-)\,\mathrm{e}^{\pi i/4}}{\sqrt{\pi w}\beta_\infty}\Big(1 - \sqrt{2kw\pi(1-\cos\theta_t)}\,\mathrm{e}^{-\pi i/4}E(k,\theta_t)\Big) \\
& + \frac{\mathrm{sgn}(\psi_t)\sqrt{k}wV(0)(P_+ + P_-)}{\sqrt{2w}\pi\beta_\infty}\sqrt{kw(1-\cos\theta_t)}\int_0^\infty \mathrm{e}^{ikw(1-\cos\theta_t)\xi}b_t(\xi)\,\mathrm{d}\xi\Bigg\} \\
& + \frac{\mathrm{sgn}(\psi)\,\mathrm{e}^{iC_\pm}\,\mathrm{e}^{ikw\sigma_t(r_t,\theta_t)}}{\sqrt{r_t}k^2(\delta - w)}\left\{\frac{\Delta p^{(t)}(0)\,\mathrm{e}^{\pi i/4}|\sin\theta_t/2|}{\sqrt{2\pi w}(\delta - w\cos\theta_t)} + \frac{\Delta p^{(t)}(0)}{\sqrt{2}}\sqrt{k}\,iE(k,\theta_t)\right. \\
& + \frac{tkA_n\,\mathrm{e}^{\pi\ i/4}w}{2\pi^{3/2}\sqrt{\delta + w}}\left(1 - \frac{(\gamma+1)M_\infty^4}{2\beta_\infty^4 w^2}(\delta - w)^2\right)\mathrm{e}^{ik(w-\delta M_\infty^2)(2+\alpha_t)+2ik\varepsilon F_R(-\infty)} \\
& \left.\Big[\mathrm{e}^{ik(w-\delta M_\infty^2)\Gamma/2+ikw\varepsilon\sigma_{l1}(2,0)}f_+(\theta_t) + \mathrm{e}^{-ik(w-\delta M_\infty^2)\Gamma/2+ikw\varepsilon\sigma_{l1}(2,2\pi)}f_-(\theta_t)\Big]\right\}
\end{aligned} \tag{C.1}$$

where

$$P_\pm = \frac{i}{\sqrt{2}}(w-\delta)P_l(0\pm)\,\mathrm{e}^{\pm ik((w-\delta M_\infty^2)\Gamma/2 + w\varepsilon V(0)\int_0^2 q(r,0\pm)\,\mathrm{d}r) + ik(w-\delta M_\infty^2)(2+\alpha_t)+2ik\varepsilon F_R(-\infty)}, \tag{C.2}$$

$$E(\theta) = \mathrm{e}^{-2ikw(1-\cos\theta)}\mathrm{erfc}\left[\mathrm{e}^{-\pi i/4}\sqrt{2kw(1-\cos\theta)}\right], \tag{C.3}$$

and

$$\begin{aligned}
f_\pm(\theta) = {} & \mathrm{e}^{\pi i/4}\frac{\sqrt{\pi}}{\sqrt{2w}}\int_0^2 \Omega(0_\pm,\tau,\tau)E\left((1-\frac{\tau}{2})k,\theta\right)\mathrm{e}^{2ikw(1-\cos\theta)}\,\mathrm{d}\tau \\
& + 2a\sqrt{k(1-\cos\theta)}\int_2^\infty \mathrm{e}^{ikw(1-\cos\theta)\xi^2/2}\left[\log[2] - \log[\xi^2/2] - \log[1-\sqrt{1-4/\xi^2}]\right]\mathrm{d}\xi \\
& + \frac{\beta_\infty}{t'}\int_0^2 \frac{\partial q^{(t)}}{\partial\theta}(r,0_\pm)\,\mathrm{d}r\sqrt{2k(1-\cos\theta)}\int_2^\infty \sqrt{1-4/\xi^2}\,\mathrm{e}^{ikw(1-\cos\theta)\xi^2/2}\,\mathrm{d}\xi \\
& - \frac{\sqrt{\pi}}{\sqrt{w}}E(k,\theta)\,\mathrm{e}^{2ikw(1-\cos\theta)}\int_0^2 \Omega(0_\pm,\tau,\tau)\frac{\mathrm{d}\tau}{\sqrt{2-\tau}},
\end{aligned} \tag{C.4}$$

with 0_- corresponding to polar angle 2π.